Stony Brook University

Synthesis of Disulfide Iron Complexes

A Thesis Presented

by

Jung-Chu Tsai

to

The Graduate School

in Partial Fulfillment of the

Requirements

for the Degree of

Master of Science

in

Chemistry

Stony Brook University

December 2011

Stony Brook University
The Graduate School

Jung-Chu Tsai

We, the thesis committee for the above candidate for the
Master of Science degree, hereby recommend
acceptance of this thesis.

Dr. Stephen A. Koch, Advisor
Professor of Chemistry

Dr. Joseph W. Lauher, Chair
Professor of Chemistry

Dr. Katherine B. Aubrecht, Third Member
Associate Professor of Chemistry

This thesis is accepted by the Graduate School

Lawrence Martin
Dean of the Graduate School

Abstract of the Thesis

Synthesis of Disulfide Iron Complexes

by

Jung-Chu Tsai

Master of Science

in

Chemistry

Stony Brook University

2011

Iron sulfur proteins are the most commonly known proteins in all living organisms. The active sites of some iron sulfur protein are clusters that are the polynuclear combinatons of iron and sulfur atoms. Iron-sulfur clusters perform various biochemical abilities, for example, electron transfer. Iron-sulfur clusters can also act as redox and non-redox catalysts. Creating model metal centers which mimic the electronic configuration of the active sites and the interaction between proteins is still an issue today. We decided to design simple and benzene thiols that imitate the side arm of cysteine (-CH_2-SH-). Therefore, we developed the H_3PS3 series ligands, one of which is H_3(PS3*).

H_3(PS3*) (Tris(3-phenyl-2-thiophenyl)phosphine) ligand contains three substituted phenyl rings that are expected to form iron complexes with different geometries because of steric effects. Through the reaction of Li_3(PS3*) with $Fe^{II}Cl_2 \cdot H_2O$ in acetonitrile, the neutral Fe(II) complex , $[Fe^{II}(PS3^*)_2]$, was obtained unexpectedly in the attempt to synthesize an Fe(II)Fe(II) dimeric complex. By studying the X-ray structure of $[Fe^{II}(PS3^*)_2]$ we suggest that the original Fe(II) ion

was oxidized to Fe(III) by unknown reasons and thus Fe(II) is regenerated by the oxidative coupling of two $(PS3^*)^{3-}$ ligands via the formation of two organic-disulfide bonds.

Table of Contents

List of Figures

List of Equations

List of Tables

Acknowledgements

I very appreciate that Dr. Koch could give me this great opportunity to work in his lab and his generosity of sharing his passion of chemistry to me. I really want to thank Soumya and Su'aad, they help me to familiar with working in the lab and are always patient to answer my questions. I learned a lot from them and they are truly great mentors. I feel thankful that Prof. Lauher and Dr. Aubrecht can be my committee and give me insctructions. I also want to thank Katherine, she is very kind to help me to do a lot paper works. And all of my friends in Stony Brook University or in Taiwan, no matter where you are, you always give me support. Finally, I want to thank my sister, she supports everything I want to do and always makes me feel optimism in my life.

Introduction

I. Iron Sulfur Proteins (Protein-Bound Iron-Sulfur)

Iron sulfur proteins are the commonly known metalloproteins in all living organisms. In the mid-1960s, iron sulfur proteins were first found as active centers of electron-transfer enzymes in which photosynthesis and respiration were involved.[1] Even though iron sulfur proteins have been known for many years, the structures of the active site are only recently becoming clear. The active sites of iron sulfur protein are called iron-sulfur clusters that are the polynuclear combinatons of iron and sulfur atoms. Iron-sulfur clusters are involved in plenty of cellular processes, such as respiration, central metabolism, gene regulation, and DNA repair and replication.[2] Iron-sulfur clusters also perform various biochemical activities.[3] For example, electron transfer, because iron-sulfur clusters have various redox states which provide a pathway of transferring electrons. Iron-sulfur clusters can also act as redox catalysts because the active sites could access both relatively high positive and low negative potentials (range from -500mV to 500mV). As non-redox catalyst, central ferric site in iron-sulfur clusters can coordinate an extensive amount of small molecule because of its own Lewis acid properties.

Studies indicate that iron-sulfur clusters are present in almost all organisms, especially in evolutionary old organisms. Furthermore, these clusters have the characteristic of being thermally stable and the property of self-assembly. In summary, iron sulfur clusters played important roles in early life on Earth. Four common types of iron sulfur clusters are shown in Figure 1.

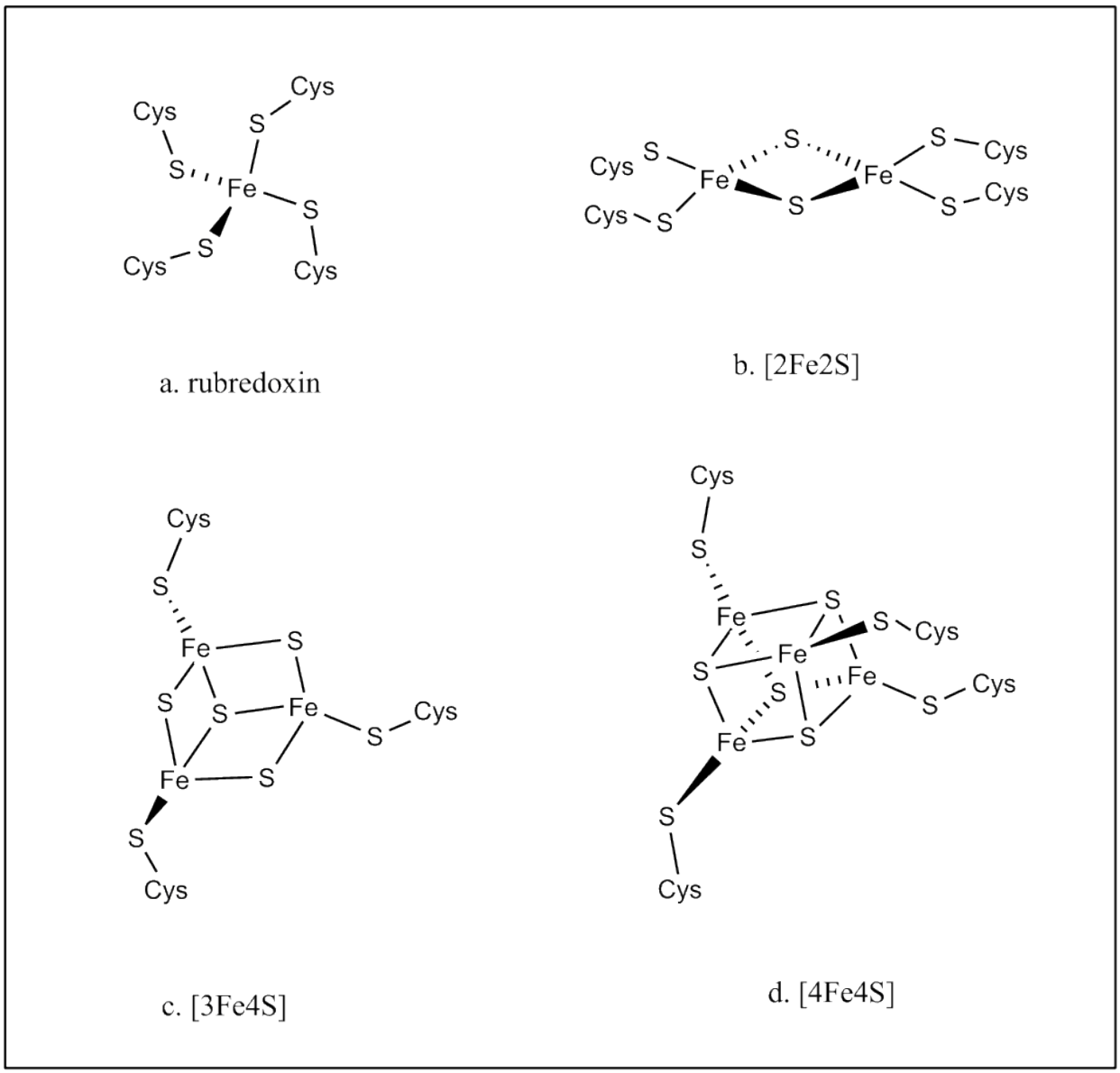

Figure 1. Structures of [Fe-S] centers in electron transfer proteins.

The stoichiometries of these centers are $FeCys_4$, $Fe_2S_2Cys_4$, $Fe_3S_4Cys_3$ and $Fe_4S_4Cys_4$ where, S represents an inorganic sulfur atom, and Cys represents a sulfur atom provided by cysteine residues. [4Fe4S] clusters are the most abundance among the four clusters.

The simplest iron sulfur cluster is called rubredoxin which contains no inorganic sulfurs and has the lowest molecular weight. The four cysteinyl groups coordinated to the iron atom with a distorted tetrahedral geometry.

The other three types of iron clusters are called ferredoxins, these clusters consist of iron-sulfur clusters in which iron atoms coordinated to cysteinyl and inorganic sulfur atoms behave as joins combining each iron atoms. [2Fe2S] clusters were discovered in chloroplasts. The structures contain two central iron atoms connected to each other through two bridging sulfur atoms, and each iron atom coordinates to two cysteine residues. Both [3Fe4S] and [4Fe4S] clusters have cuboidal geometries that [3Fe4S] clusters have an unfilled corner because of one iron less than [4Fe4S] clusters, nevertheless, each iron atom coordinates to one cysteine residue and is linked by two bridging sulfur atoms.

Most [2Fe2S] and [3Fe4S] clusters perform the only chemistry of one electron transfer. However, [4Fe4S] clusters are multi-functioned in chemistry, for example, they can act as redox catalysts and non-redox catalysts. Among the various characteristics of iron-sulfur clusters, we are interested in its access to various redox states and its wide range of redox potentials. The oxidation states of iron in monoiron clusters were determined between to be Fe(II) and Fe(III).[4] The diiron systems are Fe(III), Fe(III) in the oxidized states and Fe(II), Fe(III) in reduced states. The unpaired electron is delocalized in all the mixed-valence species. Ferredoxins have 3Fe(II), Fe(III) and 2Fe(II), 2Fe(III) redox states. One class of ferredoxins is called high potential iron

protein (HIPIP) which have unusual high oxidation potential with redox couples, 2Fe(II), 2Fe(III) and Fe(II), 3Fe(III). The following equation represents the redox states relationship between ferredoxins and HIPIP. During redox reaction, both ferredoxins and HIPIP can still provide a pathway of electron transfer because they have only little conformation changes.

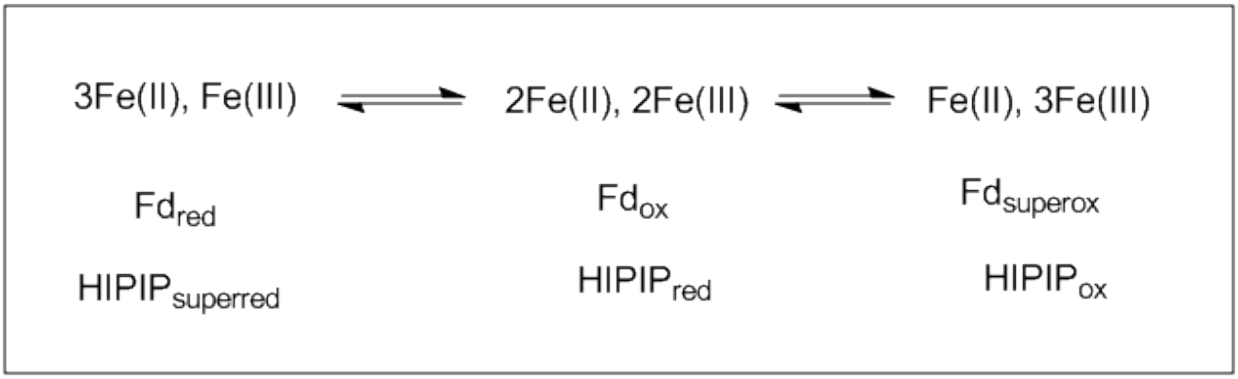

Equation 1. Redox states of ferrodoxins and HIPIP.[4]

Iron-sulfur clusters have significant interaction in hydrogenase enzymes especially [FeFe] hydroegnases that iron clusters coordinates to active site and change redox states during the catalytic reaction.

II. Hydrogenases

Hydrogen has recently been considered as an energy storage for the future world. Hydrogen is a clean source of fuel as the only by-product of combustion is water. Most of hydrogen used as fuel is produced from natural gas and oil.[5] In addition, the covalent bond energy of H_2 is 436 kJ/mol which is too high for hydrogen to be activated at room temperature and under normal pressure. Thus, producing hydrogen with an efficient way is under investigation. Scientists have been intrigued by a bacteria that can generate and uptake hydrogen in a reversible fashion,, they are called hydrogenases. Hydrogenases are metalloproteins with active sites that catalyze the reversible reaction between hydrogen and proton (eq2). [NiFe], [FeFe] and Fe-S cluster free hydrogenases[6] are the three major groups of hydrogenase enzymes[7]. We will chiefly focus on [NiFe] and [FeFe] hydrogenases here.

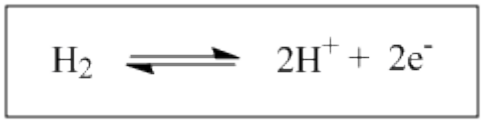

Equation 2.

A. The structure and various redox states of [NiFe] Hydrogenases

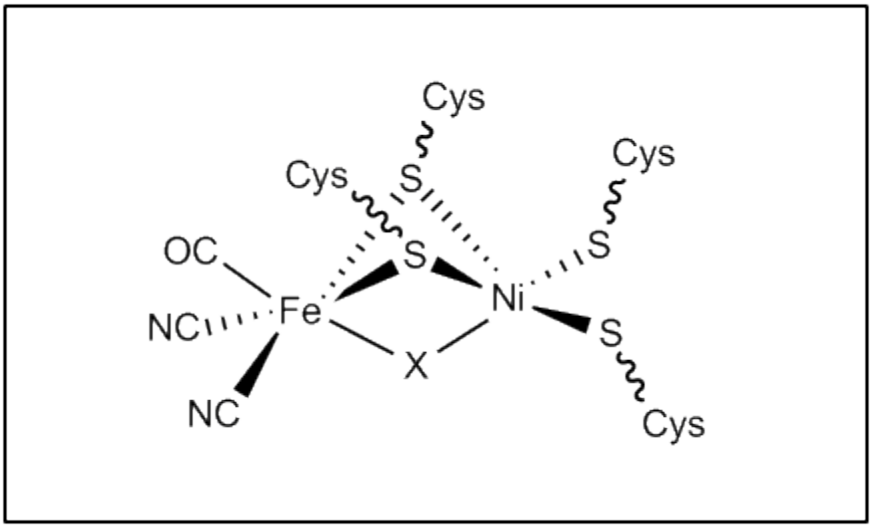

Figure 2. The strcuture of [NiFe] hydrogenase

[NiFe] hydrogenase enzyme was first crystallized from *Desulfovibrio(D) vulgaris* Miyazaki F by Higuchi et al. in 1987.[8] In the same year, another hydrogenase containing nickel and iron was also crystallized from *D. gigas* by Niviere et al.[9] The oxidized state of [NiFe] hydrogenase contains four cysteines, two of them are bridging between the two metal centers, the others are coordinated to nickel as terminal ligands in which one of the cysteines can be replaced by selenocysteine.[10] The iron atom is coordinated to two cyanides and one carbonyl ligand, which are not biological ligands. The X position in the oxidized form of [NiFe] hydrogenases might be μ-oxo, hydroxide, or sulfide ligands.[11]

Oxidized forms are classified into Ni-A (unready) and Ni-B (ready) states, and both are inactivated enzymes. Ni-A and Ni-B are distinguished by a slightly different EPR signals. Both the forms are diamagnetic (Ni^{3+}, S=1/2) states. Even in the X-ray crystal structure of *D. vulgaris*

Miyazaki F. for Ni-A state at high resolution (1.04 Å)[11a], it is hard to verify the exact arrangement of CN^- and CO ligands bound to iron atom in the active site.[12] From the X-ray diffraction studies of Ni-A state of *D. fructosovorans* hydrogenase, the bridging ligand is suggested to be peroxide species (OOH^-). According to EPR and ENDOR spectroscopic studies, the bridging molecule bound to Ni and Fe atoms should be a hydroxyl group.[13] Ni-B state could be activated under hydrogen atmosphere within a few minutes, but it takes more than an hour to activate Ni-A state because hydrogen reacts with the heterobimetallic core indirectly.[11c]

Reduction of Ni-A and Ni-B states could form Ni-SU (silent unready) and Ni-SIr (silent ready) state respectively. EPR silent state Ni-SIa (silent active) was activated from the reduction of Ni-SIr state and removal of the third bridging ligand of the active site. CO molecule could access the Ni atoms in the Ni-SIa state without other ligands blocking the way to metallic centers and therefore, CO-inhibited Ni-SCO is formed. One electron equivalent reduction of Ni-SIa produces the paramagnetic Ni-C state, in which a hydride ligand was suggested to be bridging between Ni and Fe, based on EPR studies. Ni-C was reduced to Ni-L upon illumination at low temperature. Two forms of Ni-L are called Ni-L1 and Ni-L2, which are converted at different temperature and have different EPR signals. Ni-CO is another CO-inhibited state[14] that is light sensitive and upon irradiation at low temperature results in Ni-L state.[15] The various redox states are shown in Fig. 3.

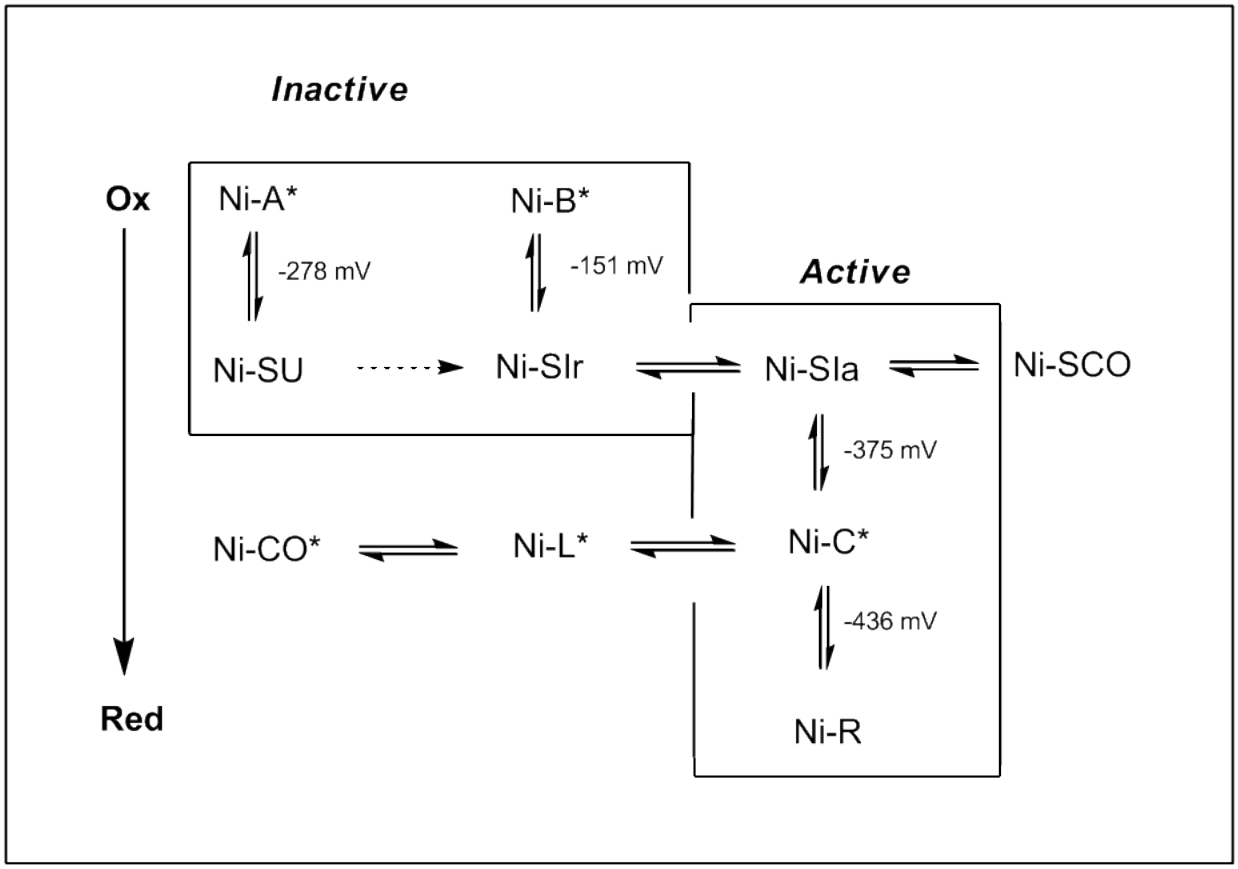

Figure 3. Schematic representation of the various redox states of the [NiFe] hydrogenase.[16] The EPR-detactable states are marked with an asterisk. The midpoint potentials measured for the [NiFe] hydrogenase from *D. vulgaris* Miyazaki F at pH 7.4 and 30^{o}C are shown against the standard hydrogen electrode. The midpoint potential of the Ni-A and Ni-SU was measured at pH 8.4 and 4^{o}C (Pandelia *et al*., unpublished data).

B. Catalytic Mechanism of [NiFe] Hydrogenases

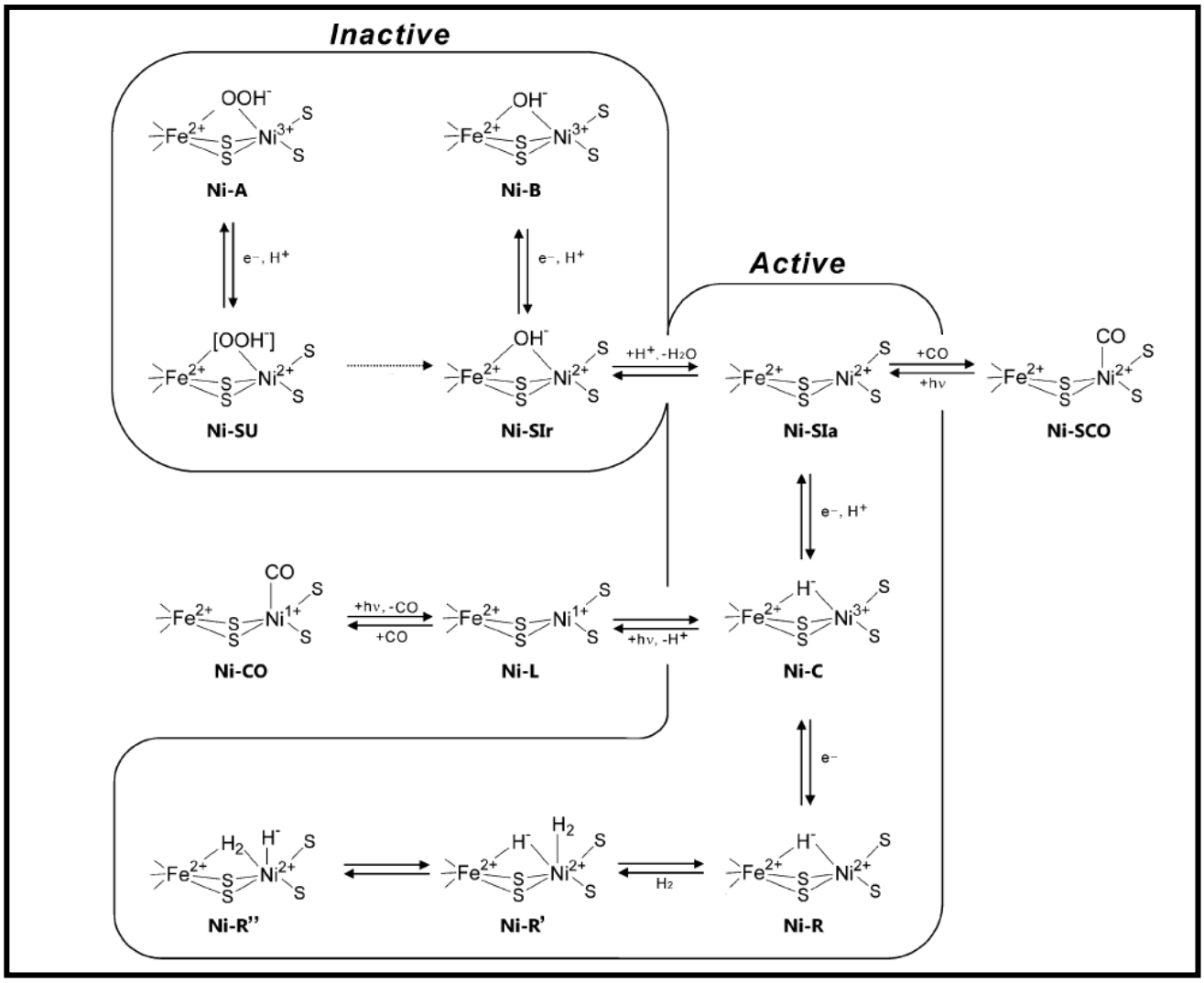

Figure 4. Proposed catalytic reaction mechanism of [NiFe] hydrogenase.[16]

From previous studies, both iron and nickel atoms are proposed to be at the active site where heterolytic cleavage takes place. The exact mechanism of the catalytic cycle has not been proven yet.[17] Ni atom was thought to be the active center where heterolytic cleavage takes place based on the experimental and computational data of biomimetic models. According to kinetic data, Ni-C, Ni-R, Ni-SIa states were considered to be involved in the catalytic cycle. During the

catalytic reaction Fe^{2+} in the active site does not change its oxidation state, while Ni has various redox states as indicated above. Ni-A and Ni-B have different EPR signals and different rates of catalyzing the reduction of H_2. The bridging ligand of the active site was assigned to [O], which might be oxygen, hydroxyl, or peroxide species. The binding position of [O] is same as that of CO in the CO-inhibited state. The bridging ligand in Ni-B was clarified to be OH^-. Reduction of overly oxidized Ni-A and Ni-B (both are Ni^{3+}) became Ni-SU and Ni-SIr respectively, which are still inactive enzyme and the bridging ligands are still present in the active sites. Protonation of bridging OH^- and removal the water in Ni-SIr leads to active Ni-SIa state (Ni^{2+}). One electron reduction of Ni-SIa formed Ni-C state, which is the central intermediate. The heterolytic cleavage of H_2 occurs here because EPR studies indicated that the hydride ligand bridge in the active site. The terminal cysteine ligand binding to the Ni of the active site was proposed as a base, which assisted the heterolytic cleavage of H_2. Additional reduction of Ni-C leads to Ni-R state and these two states are in an equilibrium with H_2. FTIR studies showed that the three subforms of the Ni-R state depend on the different protonation of the active site, and this leads to the different spin states and conformation.

C. The structures and various redox state of [FeFe] hydrogenases

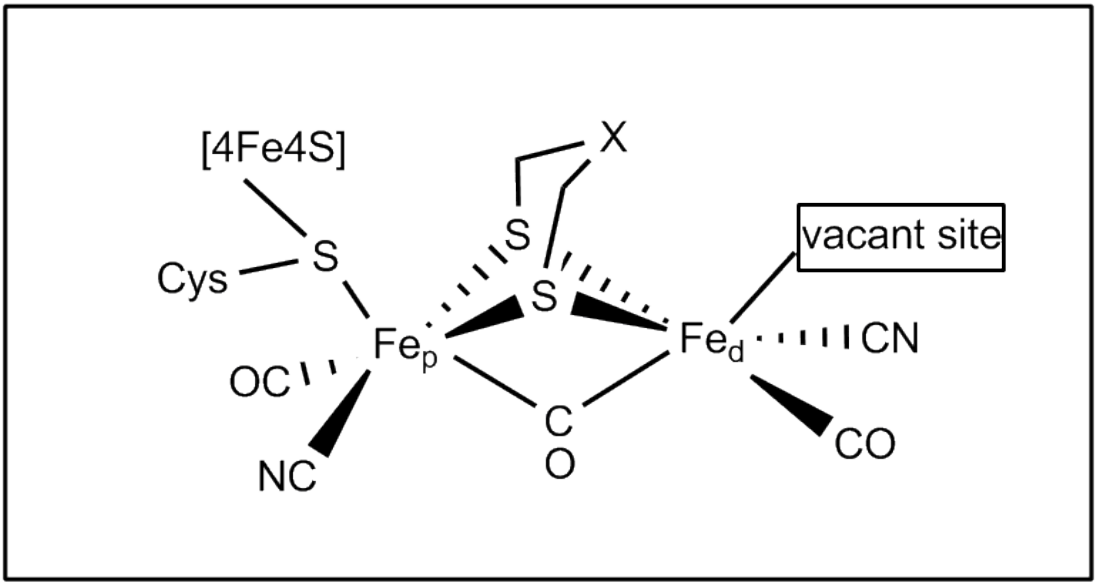

Figure 5. The structure of [FeFe] hydrogenase. (Fe_p = proximal, Fe_d = distal)

Clostridium pasterurianum was the first microorganism found without nickel in its hydrogenase enzymes.[18] The binuclear iron active site of [FeFe] hydrogenases is also called "H-cluster" which is the active center catalyzing the hydrogen evolution reaction. Only two crystallographic structures of [FeFe] hydrogenases have been studied to date. The possible structure of [FeFe] hydrogenase contains a bimetallic Fe-Fe center, a bridging ligand (SCH_2XCH_2S) bound between two iron atoms (X = CH_2, NH or O).[18] A [4Fe4S] cluster is coordinated to the active site through a cysteine thiolate from the protein backbone. Both iron atoms are coordinated to non-protein ligands; CN^- and CO[12, 19]; and a bridging CO ligand.

Two [FeFe] hydrogenases were anaerobically purified from *C. pasterianum*, Hydrogenases I and Hydrogenases II, and they are classified based on different catalytic function. Hydrogenase I is also called bidirectional hydrogenase because it can reversibly catalyze H_2 reaction.

Hydrogenase II is called "uptake" hydrogenase because it catalyzes the oxidation of H_2. Because both hydrogenases are air sensitive, these paramagnetic enzymes become diamagnetic species upon applying reductive potentials.

As studying the catalytic reaction of [FeFe] hydrogenases, [FeFe] hygrogenase in H_{inact} (H means H-cluster) state was isolated through aerobic purification from *D. vulgaris* and *D. desulfricans*. H_{inact} is diamagnetic and over-oxidized state and thus, it could be activated by reduction. FTIR studies have shown two CN^- and three CO ligands bound to iron atoms, one of the CO is a bridging ligand. Later crystallographic studies indicated the vacant site on Fe_d is coordinated to a OH^- or H_2O ligand. The two center iron atoms are of the same valence states, Fe(II)Fe(II) or Fe(III)Fe(III).

Reduction of H_{inact} formed H_{trans} state, which could be oxidized back to H_{inact} with a reversible redox reaction. Because of binding with CO and CN- ligands the iron atoms in the active site are still low spin. According to DFT calculations, oxidation states of iron atoms in the binuclear active site are Fe(II)Fe(II).[20]

By applying lower reduction potential H_{ox} state is achieved, for which Mössbauer and ENDOR studies on *C.pasteurianm* and *D. vulgaris* showed that the electron from reduction is delocalizing between the two iron atoms, i.e., Fe(II)Fe(III) or Fe(III)Fe(II). However, combining the calculated vibration frequencies from DFT and characterization of biomimetic models from FTIR features the electronic configuration of bimetallic center is Fe(I)Fe(II).[21] The ligand of the open coordination site on Fe_d is absent.

After reduction of *D. vulgaris* the H_{red} state is formed, which has one more electron than H_{ox}. Mössbauer studies assigned $[4Fe4S]_H$ in the oxidized +2 state, while for $[2Fe]_H$ cluster the oxidation state is unclear. Two postulated structures of $[2Fe]_H$ in H_{red} state are reported - one is antiferromagnetically couple Fe(I)Fe(I) state and the other one is Fe(II)Fe(II) state with a hydride ligand.[19, 22] H_{sred} is the super-reduced state that is unstable and only detected from FTIR without other spectroscopic studies to distinguish the structural and electronic details.

The H_{ox}-CO state is the CO-inhibited state of [FeFe] hydrogenases, which is found by EPR spectrum. Mössbauer and ENDOR spectroscopic studies determined that the electronic environment of H_{ox}-CO state is similar to that of H_{ox} state, Fe(II)Fe(I) and oxidized [4Fe4S] cluster.[23] A result of DFT calculation assigned the unpaired electron as being delocalized between the two iron atoms. EPR spectrum of *D. desulfricans* showed an extensive interaction of the unpaired electron with six iron atoms of both the subclusters. Because of CO binding to $Fe_{d'}$ the open coordination site is blocked causing the inhibition of hydrogenases.

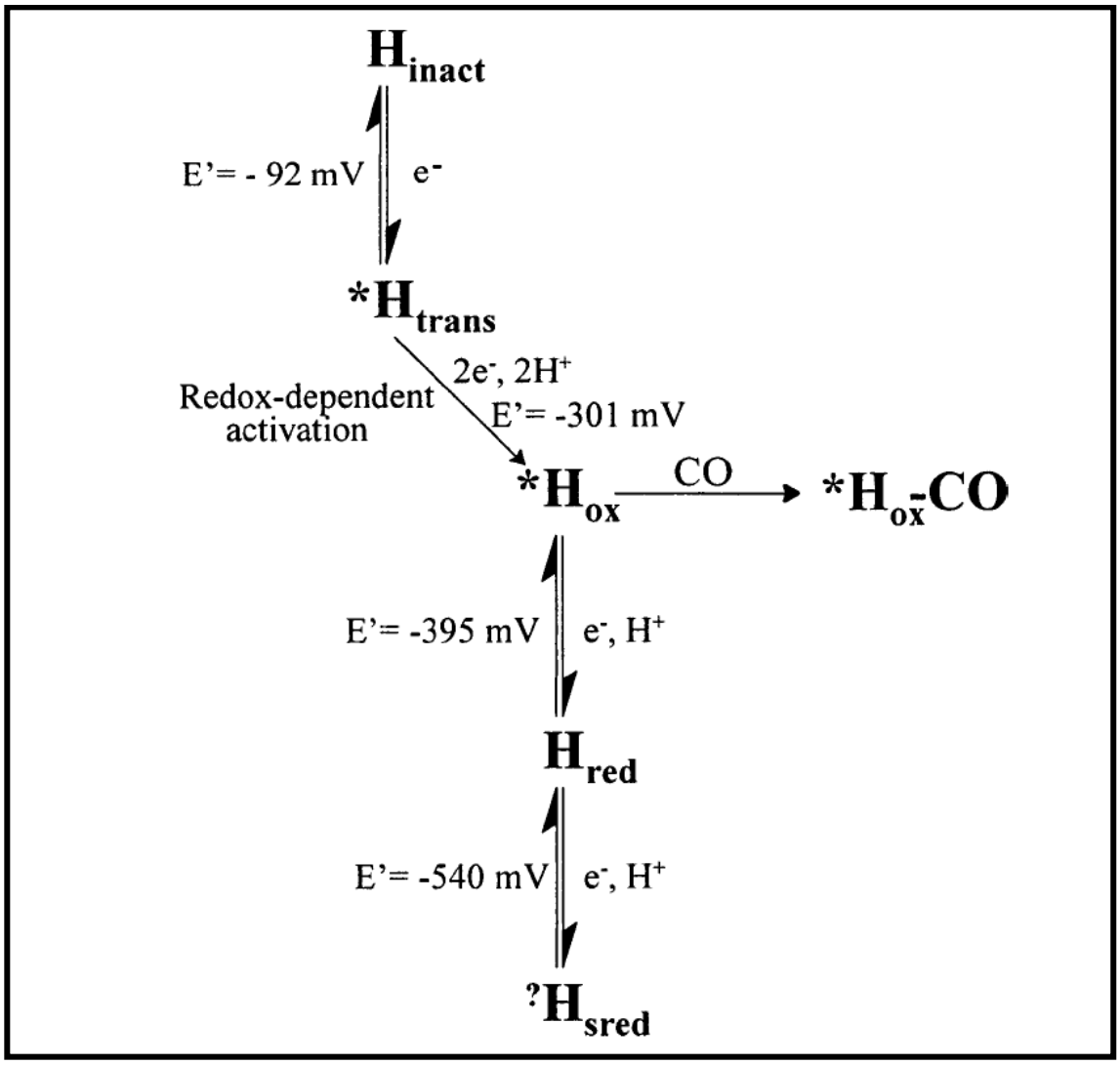

Figure 6. Schematic representation of the various redox states of the [FeFe] hydrogenase.[24] The EPR-active states are marked with an asterisk (the EPR spectra of H_{sred} have not been reported). The formal redox potentials (at pH 8.0) coorespond to those measured by FTIR-spectroelectrochemistry of *D. desulfuricans* [FeFe] hydogenase.[22]

D. Catalytic Mechanism of [FeFe] Hydrogenases

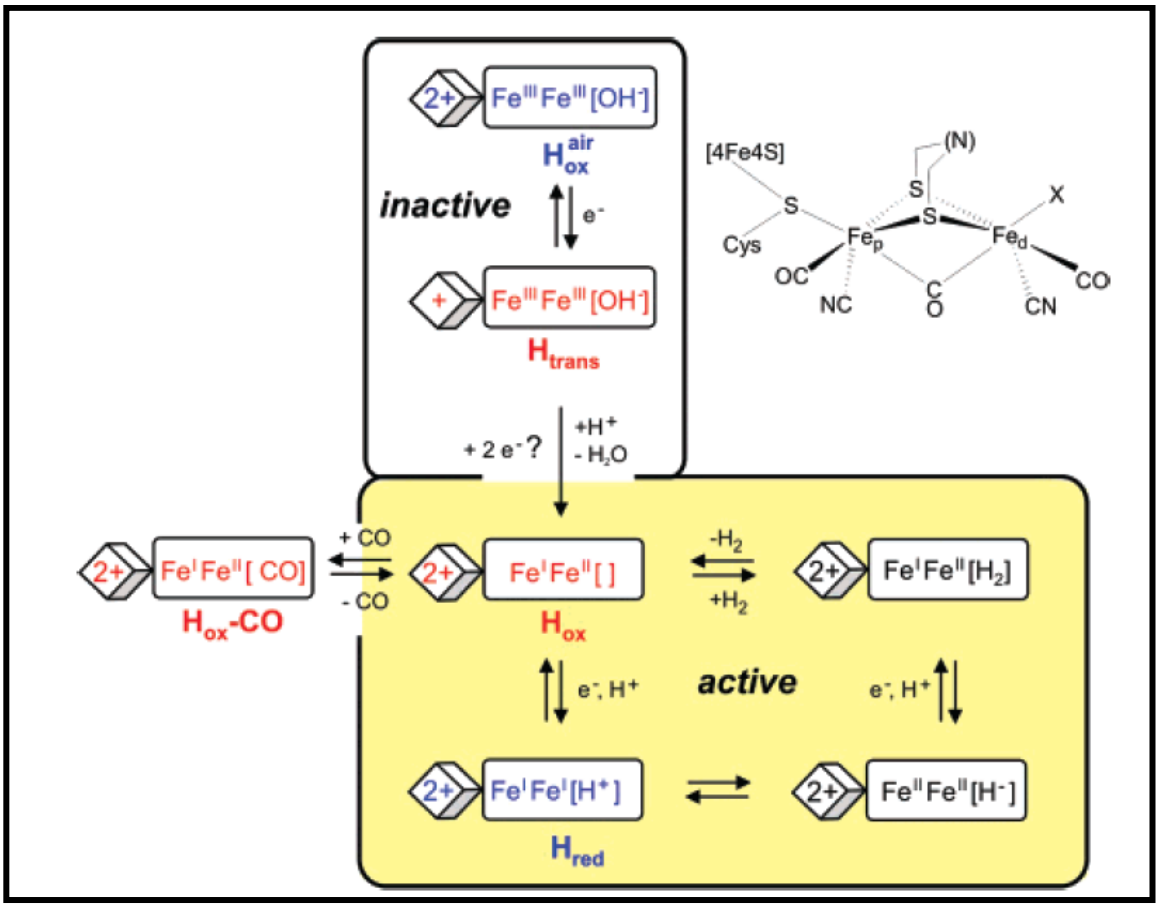

Figure 7. General scheme of redox states of the H-cluster and the proposed catalytic cycle for [FeFe] hydrogenase.[25]

In the catalytic cycle of [FeFe] hydrogenase only the computational experiments provide the elucidation of catalytic mechanism based on the combined spectroscopic studies of H_{ox} and H_{red}, the only two stable intermediates detected by the experimental methods. Fe_d of H_{ox} state is proposed to be the active site in which heterolytic cleavage of H_2 occurred, and this state is the only EPR active state, while H_2 production for the reverse reaction occurs at H_{red} state. [4Fe4S] subclusters are suggested to be electronically connected to [2Fe] cluster in which additional

electrons could be transferred to or from the [4Fe4S] subclusters during the catalytic reaction. Two hydride intermediates are proposed - hydride bound to Fe_d or hydride bridging between two iron atoms.[26] Both of them are reasonable to be catalytic models. Computational studies shows that the hydride-bridging form is thermodynamically stable and that is feasible for H_2 splitting and reduction of proton. According to FTIR and crystallographic studies, the bridging CO ligand flips toward the Fe_d and *in trans* position to the open coordination site on Fe_d during turnover. This CO ligand increases the acidity of iron and thus enhances heterolytic cleavage of H_2 and formation of terminal hydride binding to Fe_d. X-ray structure indicated that a substrate (H_2) is coordinated to the open site of Fe_d and competing with CO (inhibitor). However, the structure of hydride bound to the active site is yet to be found. To investigate the sophisticated mechanism, we need advance spectroscopic techniques to examine the electronic configuration of the intermediates.

Results and Discussion

Creating model metal centers that mimic the electronic configuration of active sites and interaction between proteins is still an issue today. Cysteine exists in both [NiFe] and [FeFe] hydrogenases, and it is generally considered as a model ligand to imitate. The problem of using cysteine is that it forms oligomeric compounds easily because of its tendency to bridge metals. But experiments showed that, sulfur-containing amino acid (methionine or cysteine) reacted with Pt(II)[27] by HSAB theory (Hard and Soft Acids and Bases). Because Pt(II) complexes with cysteine ligands were successfully isolated, we decided to design simple thiols, benzene thiols, that imitated to the side arm of cysteine (-CH_2-SH-). Again the problem of utilizing cysteine is leading the results of oligomeric compounds but monomeric metal-cysteine complexes do exist. In addition, thiolates can act as reducing agent; reacting high valent metal centers through an auto-redox reaction to form the reduction form of metal and sulfide (Equation 3). However, there are numerous examples of stable high-valent metal center proteins.

$2M^{n+} + 2RS^{-} \rightarrow 2M^{(n-1)+} + RSSR$ (Equation 3)

In order to prevent formation of oligomeric compounds and auto-redox reaction of high valent metal and thiolates, increasing the steric effect of the thiol ligands can prevent the problems as mentioned. Furthermore, Wilkinson has reported that chelate effects of polydentate ligands can stabilize metal complexes.[28] Due to all of the considerations, we decide to design tripodal ligands. Dr. Nguyen[29] in Millar group developed the H_3PS3 series ligands, shown in Figure 8.

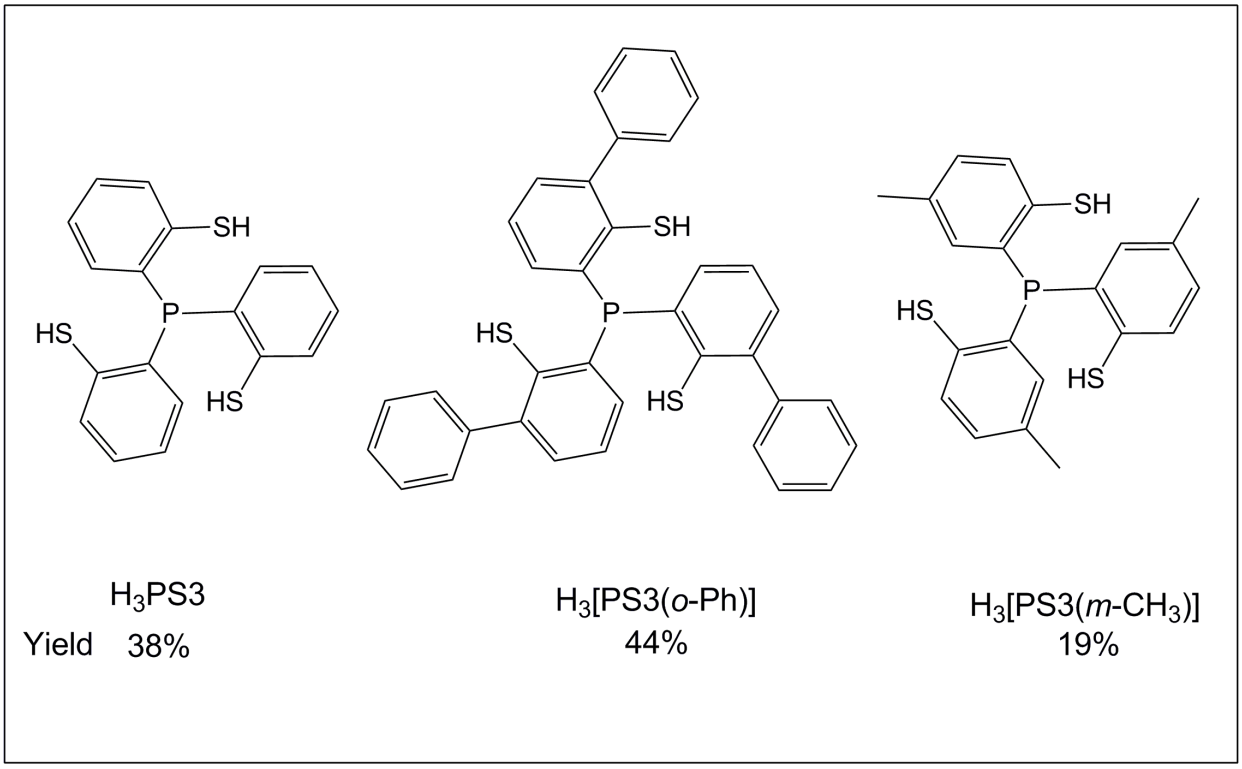

Figure 8. Polythiolate ligands and yields of products.

The first H_3PS3 ligand is tris(*o*-benzothiolate)phosphine ligand which is synthesized via ortho-lithiation of thiophenol followed by the appropriate electrophile. Later $H_3[PS3(o\text{-}CH_3)]$ [tris(5-methyl-2-thiophenyl)phosphine] and $H_3[PS3(o\text{-}Ph)]$ [tris(3-phenyl-2-thiophenyl)] were developed, both followed the same procedures as H_3PS3 but used different thiobenzenes.

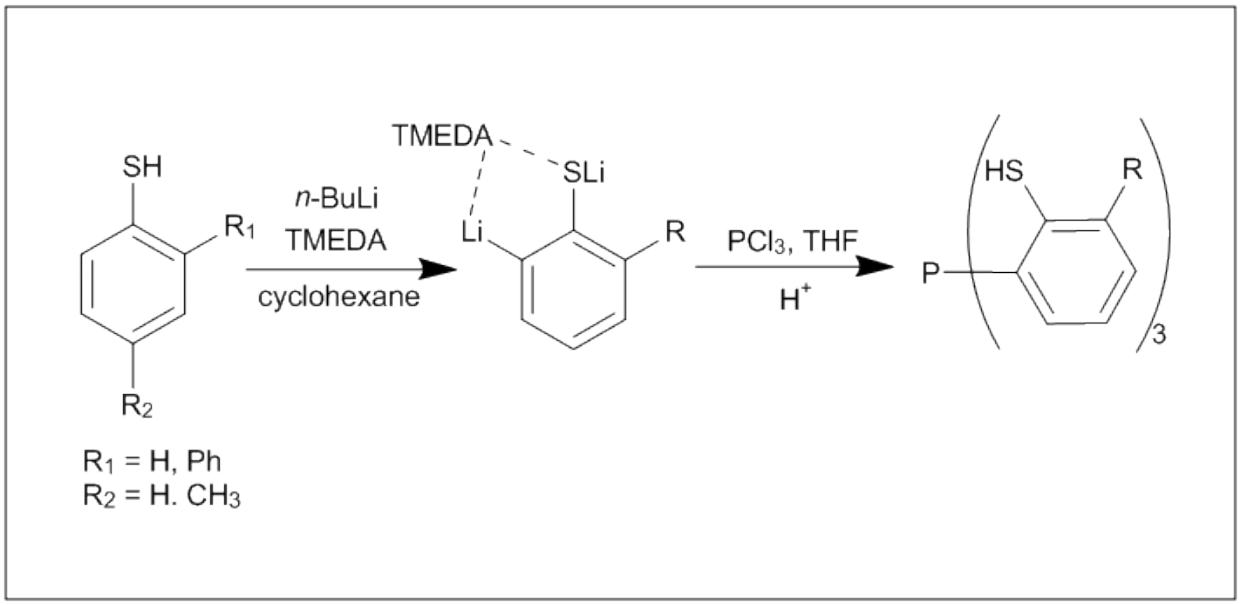

Figure 9. Synthetic pathway to PS3 and its derivatives.

Because H_3PS3 resulted in dimeric complexes, H_3[PS3(*o*-Ph)] which consists of three substituted bulky phenyl rings is expected to give monomeric complexes with metal centers. Three phenyl rings also create a complex with a cavity where chemistry can be achieved with the cavity at the axial position (Figure 10).

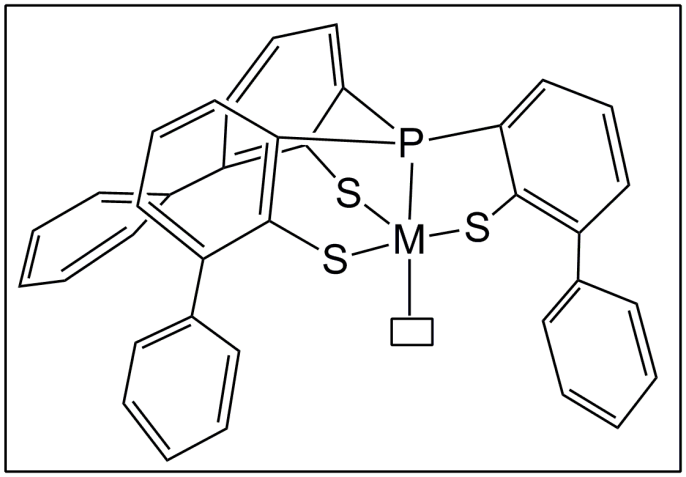

Figure. 10 A five-coordinate metal complex of H_3[PS3(*o*-Ph)].

The precursor of H_3[PS3(*o*-Ph)] is 2-phenylbenzenethiol which was published by Eisch in 1978.[30] Here 2-phenylbenzenethiol is prepared by a different methodology.[31] 1,1'-biphenyl-2-amine is dissolved in water, and then hydrochloric acid was added at 0°C. Sodium nitrite was dissolved in water and added to the reaction mixture slowly. After stirring 30 minutes, sodium salt of diethyldithiocarbamic acid trihydrate was then added into solution at 45°C. After extracting from diethyl ether, an oil product of S-2-benzylphenyl-diethyldithiocarbamic acid was received. A tetrahydrofuran solution containing lithium aluminum hydride and S-2-benzylphenyl-diethyldithiocarbamic acid (**1**) was refluxed for 18 hours, then quenched with ethyl estate and subsequently sulfuric acid was added to pH 3. The solution was extracted with diethyl ether, and washed with sodium hydroxide solution. After the reduction reaction, we supposed to obtain 2-phenyl benzenethiol, however, according to X-ray structure and NMR spectrum we still obtain the same starting material, S-2-benzylphenyl-diethyldithiocarbamic acid. It is hard to grow crystals from the oily **1** compound, but after refluxing with reducing agents, the crystals were obtained easily. We suggest that the oily compound **1** contains impurities that consumed reducing agents during the reaction, so that we received the pure products **1**. While replacing thiols with compound **1** as starting materials of the synthesizing reaction of H_3[PS3(*o*-Ph)], we still obtain the H_3[PS3(*o*-Ph)] ligand. We usually use excess *n*-BuLi in the lithiation reaction, and butyl group is strong nucleophile that could donate its electrons to the carbamoyl group and thus formed as a leaving group that is leaving from the thiolate of the phenyl group. Therefore the lithium complex is formed and performed the same procedure of PS3 Ligand series. The mechanism of lithiation is Figure 11b, three equivalent of *n*-BuLi is supposed to be used in this reaction.

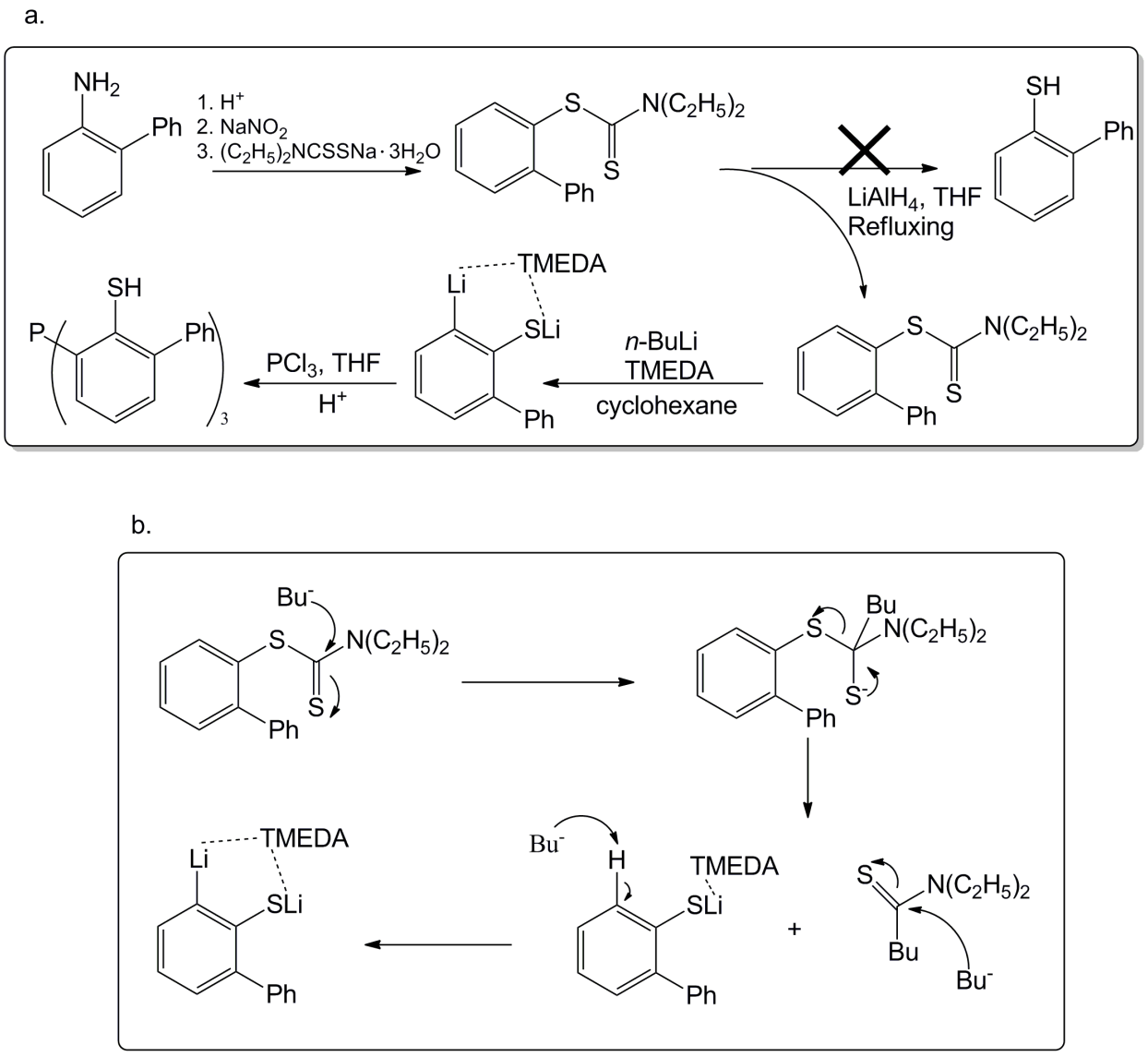

Figure. 11 a. Reaction scheme of compound **1** and different methodology of synthesizing H_3[PS3(*o*-Ph)] ligand. b. Proposed mechanism of lithiation of compound **1**.

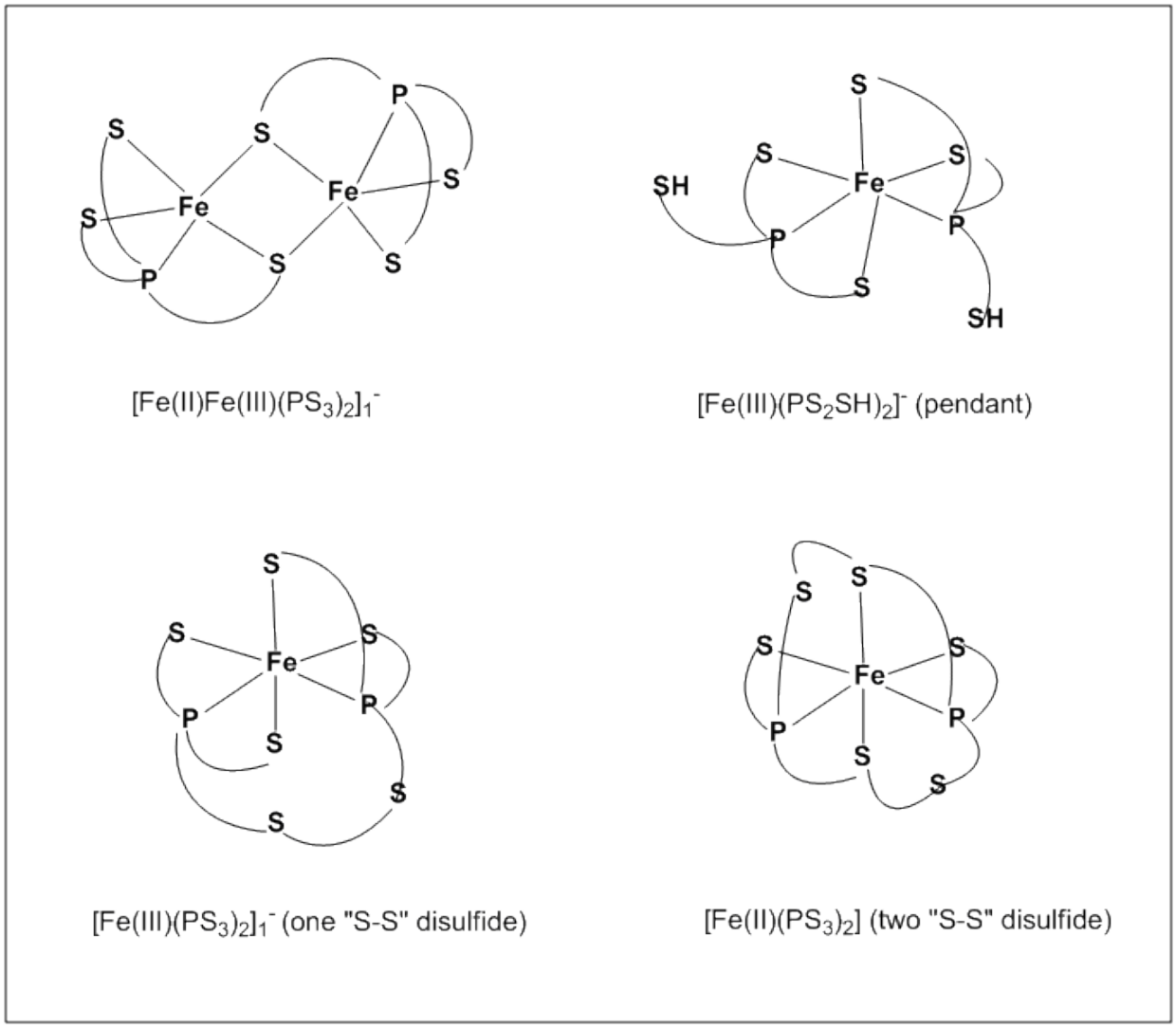

Figure 12. Some examples of Fe-PS3 complexes[32]

H_3PS3 ligands has been studied with iron metal by Koch and Millar group for years. In the past we have synthesized various iron complexes of the PS3 ligands series (Figure 12). For H_3[PS3(*o*-Ph)] ligand, Hsu and Nguyen focused on $\{Fe^{II/III}[PS3(o\text{-}Ph)]\}^{n-}$ and $\{Ni^{II/III}[PS3(o\text{-}Ph)]_n\}$ (n =1 or 2) complexes, respectively. Here we want to isolate a monomeric oxygen-binding iron complex with $[PS3(o\text{-}Ph)]^{3-}$ ligand due to the steric effects of the three bulky phenyl rings

(Figure 13a). Therefor oxygen was added to an acetonitrile solution containing Li_3[PS3(*o*-Ph)] and $FeCl_2$•$2H_2O$. The solution became black as soon as oxygen was added. The solvent was evaporated under vacuum after the addition of tetraphenyl phosphoninum cation. The black residues were dissolved in dichloromethane and layered with diethyl ether at room temperature for two days. The black needle-like crystals were grown from the mixture. Because the diffraction of the crystals is not good enough, we cannot obtain the X-ray structure.

a.

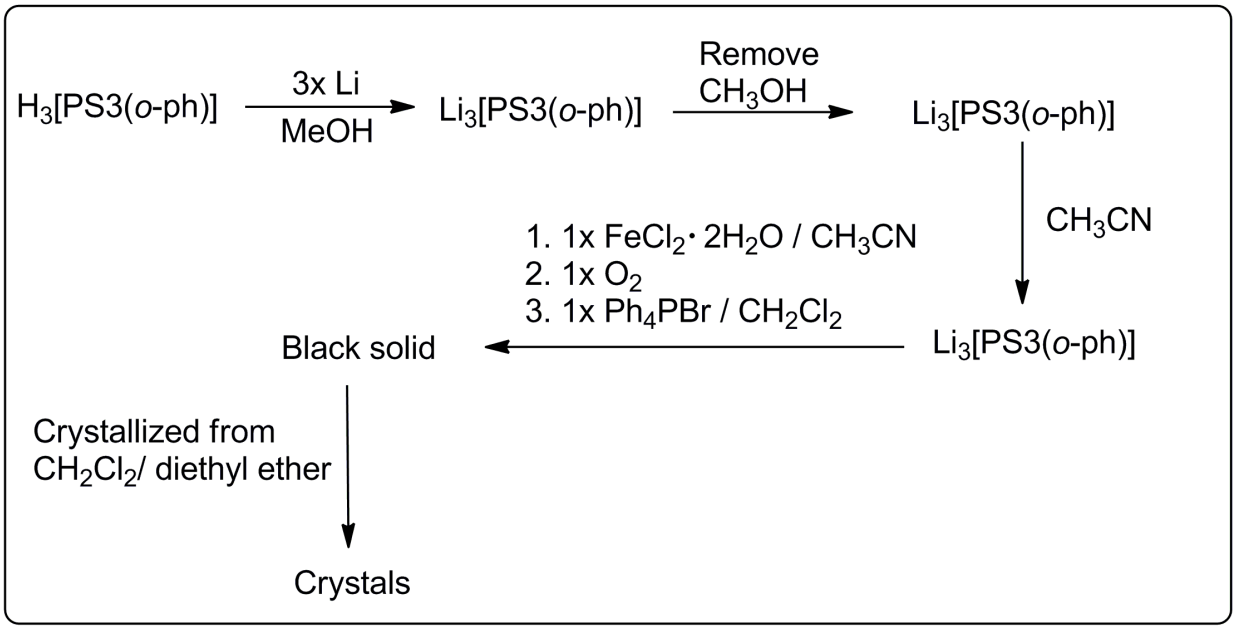

b.

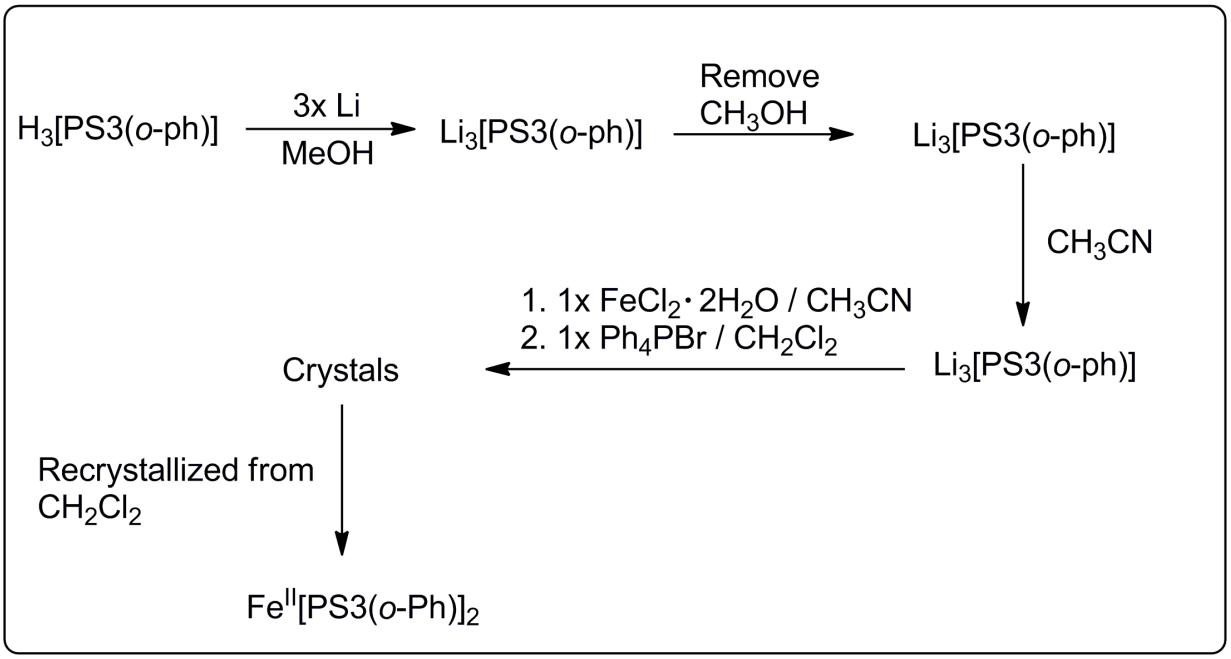

Figure 13. The reaction scheme of synthesis of iron complexes of $[PS3(o\text{-Ph})]^{3-}$ ligands. a. Synthesis of iron complexes of $[PS3(o\text{-Ph})]^{3-}$ ligands with O_2. b. Synthesis of iron complexes of $[PS3(o\text{-Ph})]^{3-}$ ligands.

Based on our studies of iron complexes binding to PS3 ligands, we believe that the $[Fe^{II}Fe^{II}(PS3)_2]^{2-}$ complex does exist. By layering the reaction mixture of $Li_3[PS3(o\text{-}Ph)]$ and $FeCl_2 \bullet 2H_2O$ on the dichloromethane solution of tetraphenyl phosphoninum cation for 3 days, we received black cubic crystals (Figure 13b). These crystals were attempted to be analyzed by X-ray diffraction for many times, but even at 100K they decayed quickly, so that we could not receive the crystallographic data. We also tried growing crystals in acetonitrile without dichloromethane solvent since that dichloromethane may be constituted in the crystals and be evaporated quickly thus causing the crystal to decay. However, we still could not to obtain the X-ray structure. Therefore the crystal residues were recrystallized from slowly evaporation in dichloromethane. After two days, black crystals were isolated, that were shown to be $Fe^{II}[PS3(o\text{-}Ph)]_2$. $Fe^{II}[PS3(o\text{-}Ph)]_2$ is a neutral complex without any cation in the crystal cell. $Fe^{II}[PS3(o\text{-}Ph)]_2$ is a six coordinate complex with two $[PS3(o\text{-}Ph)]^{3-}$ ligands. Iron is bound to both phosphine and one thiolate from each $[PS3(o\text{-}Ph)]^{3-}$ and also to the two disulfide that formed during the reaction. This means that the oxidation state of iron atom has to be Fe^{2+}. Forming a disulfide bond from thiolates releases two electrons therefore four electrons are released when two disulfide bonds are formed. Franolic[32b] obtained $[Fe^{II}(PS3)_2]$ complex using Fe(III) as starting material previously (Figure 16). But now we performed this reaction with Fe(II). The result suggests that as least two redox reaction occurred during reaction; the original Fe(II) was oxidized to Fe(III) by accidental oxygen, and thus Fe(III) was reduced back to Fe(II) by the electron freed from forming the disulfide bond.

The X-ray structure of $Fe^{II}[PS3(o\text{-}Ph)]_2$ is illustrated in Figure 14 and 15. The significant features of the structure is that the central Fe(II) is coordinated by two six-membered rings and four five-membered rings. The six-membered rings contain a disulfide bridge that link two

[PS3(*o*-Ph)]$^{3-}$ ligands. Two phosphine atoms are in a *cis* position to each other; in addition, two thiolates are also *cis* to each other. The two sets of phosphine and thiolate atoms are in the same equatorial plane. P1-Fe1-P1 bite angle is 101.18 (4)^{o}, which makes the octahedral geometry slightly distorted. The bond distances of Fe(II)-disulfide (2.2019 (6) **Å**) are shorter than that of Fe-thiolate distances (2.3287 (7) **Å**), that might be caused by π donation from S1 to iron atom. The S-S distances are the normal values in organic disulfide bond. (Table 1)

Table 1. Selected Bond Distances and Bond Angles for $Fe^{II}[PS3(o\text{-}Ph)]_2$

Bond Distances (Å)	
Fe(1)-P(1)	2.1340(7)
S(2)-S(3)*	2.1179(8)
Fe(1)-S(1)	2.3287(7)
Fe(1)-S(2)	2.2019(6)
Bond Angles (°)	
P(1)*-Fe(1)-P(1)	101.18(4)
P(1)-Fe(1)-S(1)	84.97(2)
P(1)-Fe(1)-S(2)	88.76(2)
S(2)*-Fe(1)-S(2)	177.29(4)
P(1)-Fe(1)-S(1)*	173.58(3)
S(2)-Fe(1)-S(1)	85.27(2)
P(1)-Fe(1)-S(2)*	92.96(2)
S(2)-Fe(1)-S(1)*	92.79(2)

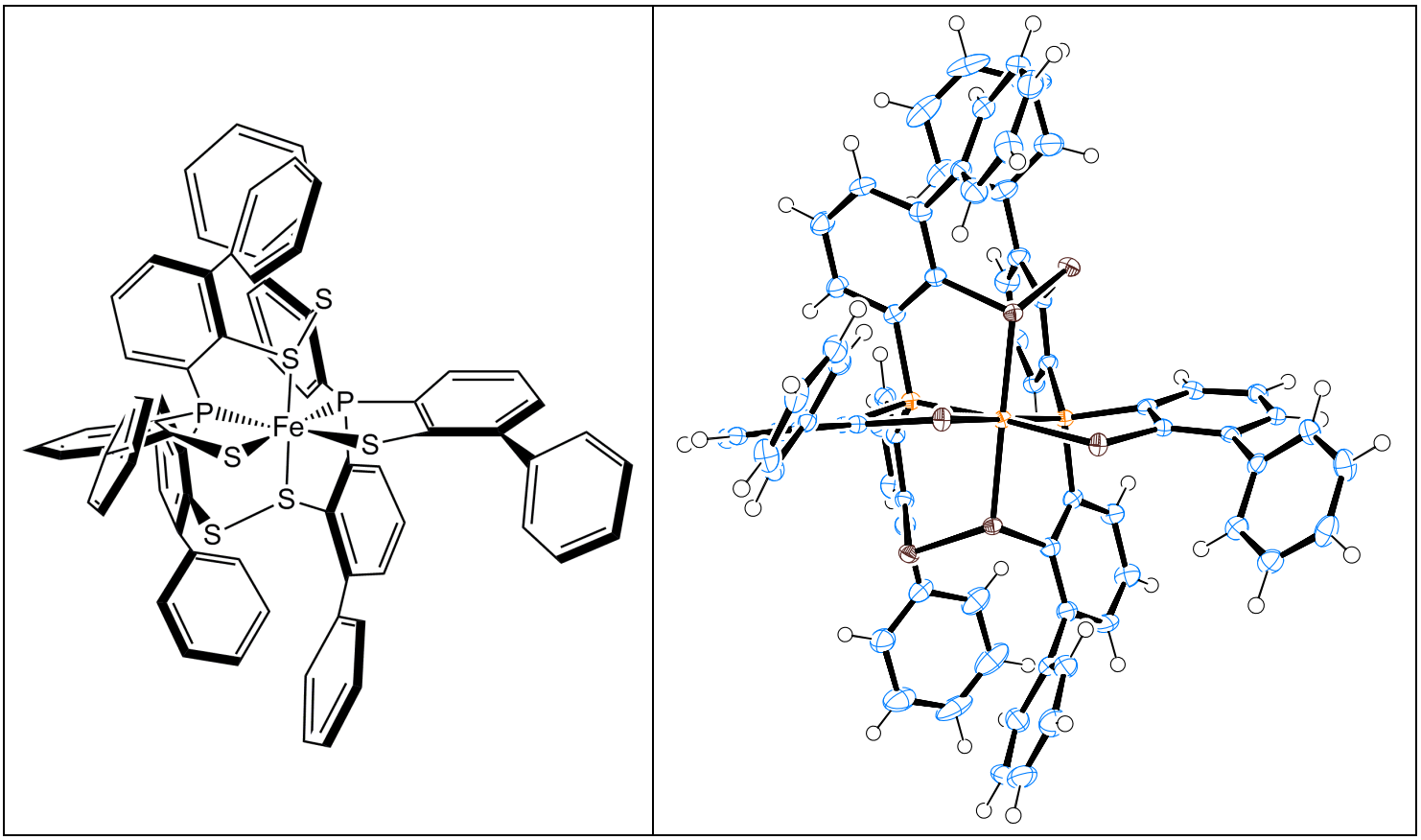

Figure 14. Ortep X-ray structure of $Fe^{II}[PS3(o\text{-}Ph)]_2$

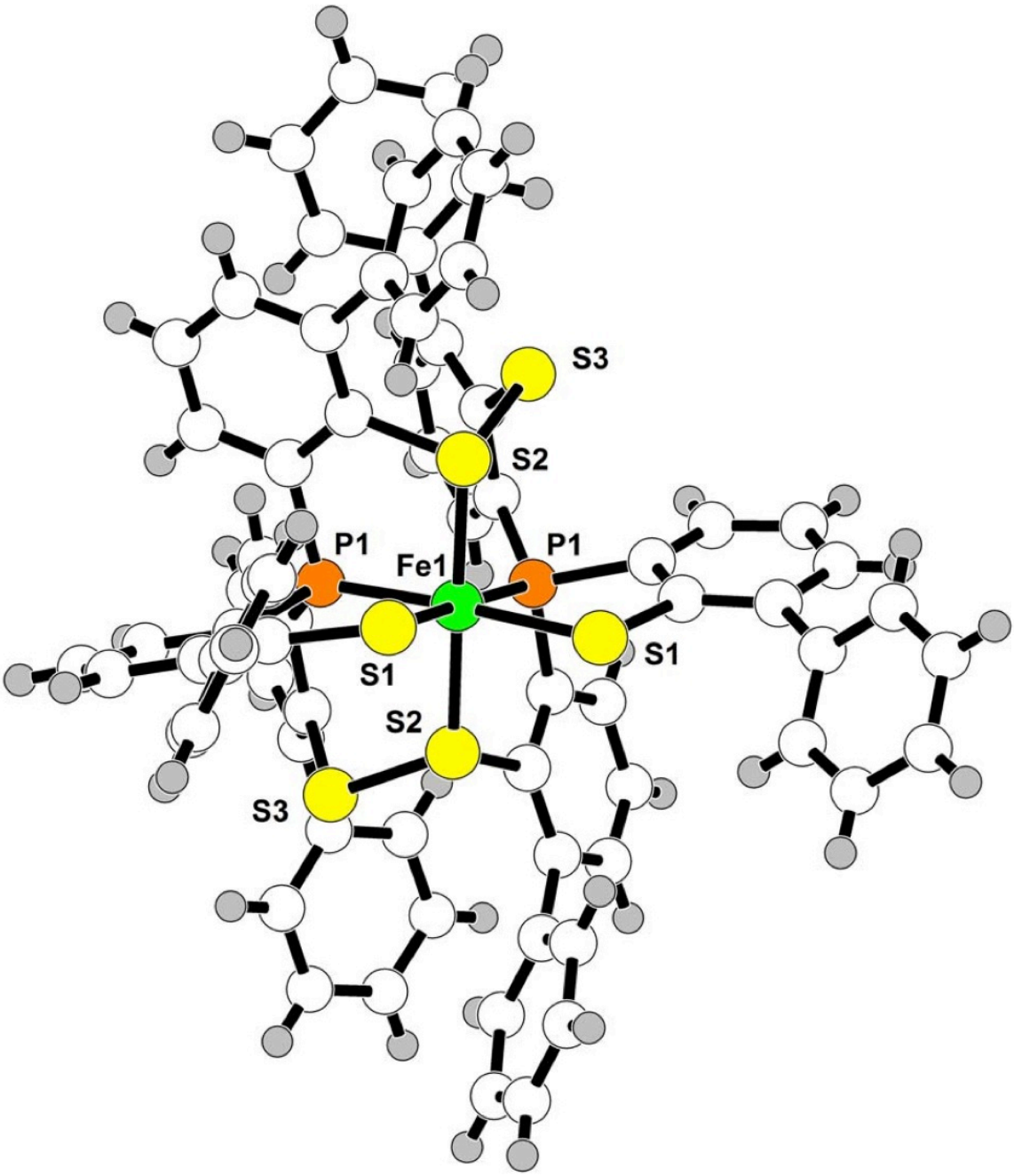

Figure 15. CHARON diagram of $Fe^{II}[PS3(o\text{-}Ph)]_2$

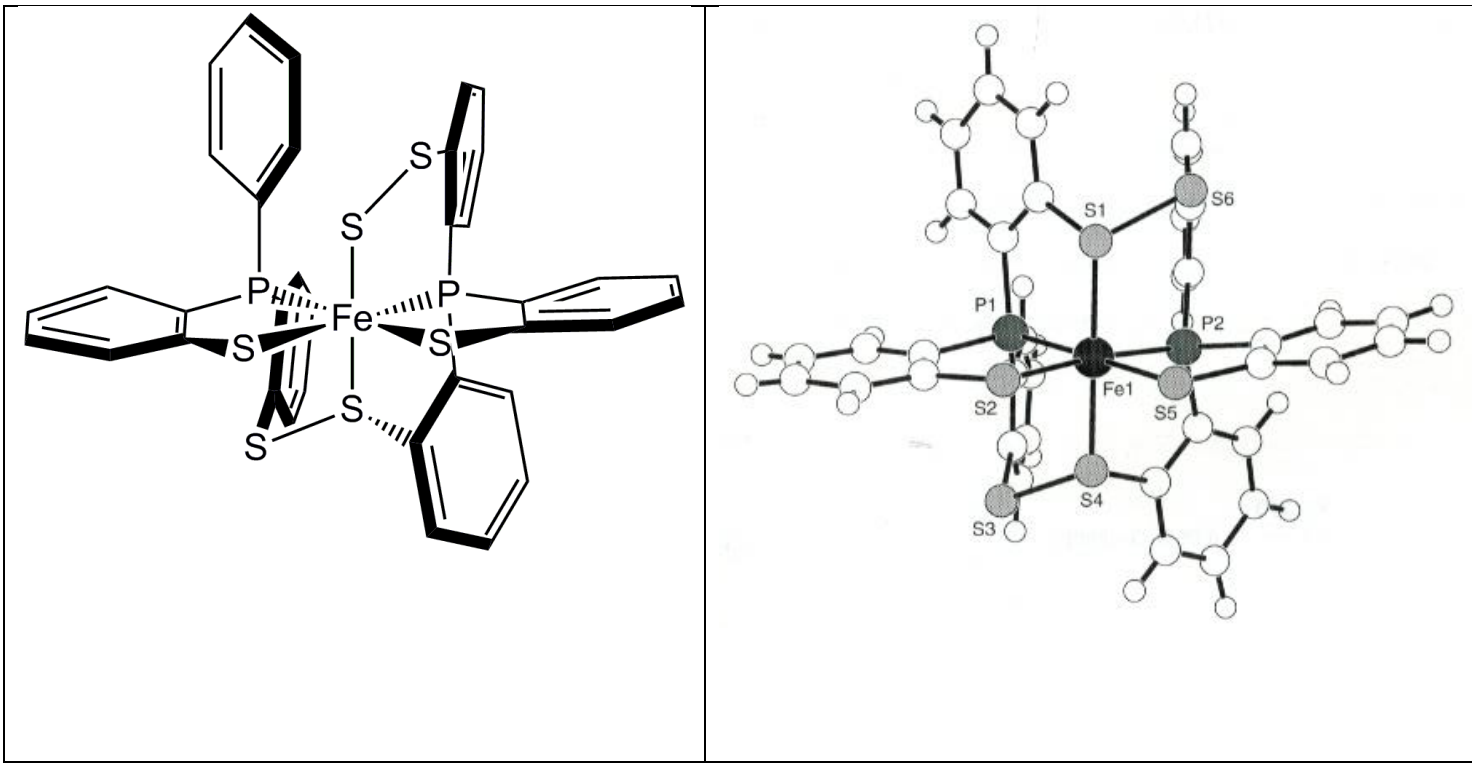

Figure 16. CHARON diagram of $Fe^{II}(PS3)_2$[32b]

Conclusions

Isolating the oxidized Fe(II)Fe(II) complex of H_3[PS3(*o*-Ph)] ligand could stimulate the understanding of oxygen activity with Fe(II) complexes. Elucidating the mechanism of the formation of disulfide bond in the Fe^{II}[PS3(*o*-Ph)]$_2$ helps us to understand the redox chemistry of iron center, in addition, that could be explained as a potential catalytic activity of the central iron. Fe^{II}[PS3(*o*-Ph)]$_2$ is the first iron complex with bis**-**tris(3-phenyl-2-thiophenyl)phosphine ligand, we expect to synthesize monomeric and dimeric iron complexes of [PS3(*o*-Ph)]$^{3-}$ ligands and to discuss more chemistry of metal complexes with [PS3(*o*-Ph)]$^{3-}$ ligands in future.

Experimental Techniques

Synthetic Techniques

All reactions were performed under standard Schlenk conditions under a nitrogen atmosphere. All air-sensitive solids were transferred to other medium via a glove box, also under a nitrogen atmosphere.

Instrumentation

NMR Spectroscopy

All ^{1}H NMR spectroscopy were recorded on a Varian Gemini 2300 spectrometer at 300 MHz. All spectra were taken in deuterated solvent and reported in units of parts per million (ppm).

X-Ray Crystallography

All reported X-ray crystallography studies were performed with an Oxford Diffraction Gemini Diffractometer, utilizing Molybdenum radiation. Some structures were done at low temperature and is indicated in the individual compound data located in the appendix. Data reduction was performed with CrysalisPro software, and the structures were solved using Wingx, Shelx and SIR2004.

Synthesis

S-2-benzylphenyl-diethyldithiocarbamic acid

Concentrated hydrochloric acid (8 mL) was slowly added into a water solution (80 mL) containing [1,1'-biphenyl]-2-amine (5 g, 0.03 mole) at 0^oC and the reaction mixture was stirred for 30 minutes. Sodium nitrite (2.44 g, 0,035 mole) was diluted with water (15 mL) and added slowly into the reaction mixture at 0^oC. After stirring for 30 minutes, the solution was warmed up to 45^oC and then the water solution (20 mL) of diethyldithiocarbamic acid sodium salt trihydrate (8.16 g, 0.04 mole) was slowly added. After an hour stirring, the reaction mixture was cooled to room temperature. The solution was extracted with diethyl ether 3 times (100 mL x 3) and the organic layer was separated and washed by sodium hydroxide (10 M) solution twice and once with brine. The organic layer was dried over sodium sulfate and filtered. Evaporating all the solvent gave the red oily product. After refluxing the oily product and $LiAlH_4$ in THF, the resulting yield is 3.0 g, 33%.

^1H NMR ($CDCl_3$): δ 1.20 (m, 6H, CH_3), δ 3.86 (dd, 4H, CH_2), δ 7.32-7.63 (m, 9H, CH)

Tris(3-phenyl-2-thiophenyl)phosphine, H_3[PS3(*o*-Ph)]

TMEDA (5.2 mL, 0.021 mol) was cannulated into 2.5 M *n*-BuLi (13.8 mL. 0.021 mol) in cyclohexane. A solution of S-2-benzylphenyl-diethyldithiocarbamic acid (2.90 g, 0.01 mole) in

75 mL of cycloheaxane was added dropwise to this solution at 0°C. The mixture gradually came to room temperature and was stirred for 18 hours. The resulting yellow slurry was filtered on a Schlenk frit, washed with cyclohexane, and dried in vacuum. The dilithium salt-TMEDA complex (2.11 g, 0.007 mole) was dissolved in THF. This solution was cooled to -78°C and treated dropewise with PCl_3 (0.31 g, 0.0022 mole) in THF. The mixture was the allowed come to room temperature and stirred for 18 hours.

After acidifying the solution to pH 6 with 10% H_2SO_4, it was opened to air. The layers were separated and the aqueous layer was extracted with diethyl ether. The combined organic layer was washed with water and brine. Since the product can begin precipitating out of solution during work up, no drying agent was used so that product would not inadvertently be removed when filtering out the drying agent.

As some of the solvent was allowed to evaporate, several grams of white solid precipitated out of solution. This product was filtered and washed with cold (-20 °C) methanol. Subsequent crops were collected from the gummy solid left after all the solvent had evaporated, and were recrystallized from dichloromethane/ methanol, filtered, and washed with cold methanol. Total product is 23% yield.

This is experiment record, the theory stoichiometry should be, S-2-benzylphenyl-diethyldithiocarbamic acid (1x); TMEDA (2.2x); *n*-BuLi (3x).

^{1}H NMR ($CDCl_3$): δ 4.42 (s, 3H, SH), δ 6.9-7.5 (m, 24H, CH)

$Fe^{II}[PS3(o\text{-}Ph)]_2$

Methanol solution containing of H_3[PS3(*o*-Ph)] (120 mg, 0.2 mmol) and Lithium wire (4.2 mg, 0.6mmol) was stirred for 10-15 minutes. After Evaporating all the methanol solvent under vacuum, the solid residue was dissolved in acetonitrile and was added slowly to an acetonitrile solution of $FeCl_2 \cdot 2H_20$ (34 mg, 0.21 mmol). Immediately, a green solution formed. After stirring for 15-20 minutes, the solution was filtered through celite under N_2. Then the solution was layered onto dichloromethane solution of tetraphenyl phosphonium bromide and kept at room temperature for 3 days as the dark green crystals form. The quality of the dark green crystals is not good enough for X-ray diffraction. The crystals were re-dissolved in dichloromethane again for slowly evaporation. Dark red crystals grow in three days. The results of X-ray structure was an unexpected result of Fe^{II} $[PS3(o\text{-}Ph)]_2$.

Fe^{II} [PS3(*o*-Ph)]O

Methanol solution containing of H_3[PS3(*o*-Ph)] (120 mg, 0.2 mmol) and Lithium wire (4.2 mg, 0.6 mmol) was stirring for 10-15 minutes. After Evaporating all the methanol solvent under vacuum, the solid residue was dissolved with acetonitrile and was added slowly to an acetonitrile solution of $FeCl_2 \cdot 2H_20$. The reaction mixture became a green solution right away. After stirring for 15-20 minutes, one equivalent of oxygen produced by $FeCl_3$ and H_2O_2 was added into the solution. A brown-red solution appeared. The mixture was stirred for 30 minutes and filtered through celite under N_2. The filtrate was layered on dichloromethane solution of tetraphenyl phosphonium bromide. Evaporated all the solvent gave dark solids which are then dissolved in

dichloromethane with diethyl ether layer on its top. Red needle-like crystals were received next day, but these crystals did not have good quality for X-ray diffraction.

References

1. (a) Beinert, H., Iron-sulfur proteins: ancient structures, still full of surprises. *Journal of Biological Inorganic Chemistry* **2000,** *5* (1), 2-15; (b) Kaim, W. S., B In *Bioinorganic Chemistry; Inorganic Elements in the Chemistry of Life,* **1994**, *1st Ed*., 128-139.

2. Fontecave, M., Iron-sulfur clusters: ever-expanding roles. *Nat Chem Biol* **2006,** *2* (4), 171-174.

3. Py, B.; Barras, F., Building Fe–S proteins: bacterial strategies. *Nat Rev Micro* **2010,** *8* (6), 436-446.

4. Crabtree, R. H., The Organometallic chemsitry of the transition metal **2009,** *5th Ed,* 465-466.

5. Thauer, R. K., Hydrogenases and the Global H2 Cycle. *European Journal of Inorganic Chemistry* **2011,** *2011* (7), 919-921.

6. Lyon, E. J.; Shima, S.; Buurman, G.; Chowdhuri, S.; Batschauer, A.; Steinbach, K.; Thauer, R. K., UV-A/blue-light inactivation of the 'metal-free' hydrogenase (Hmd) from methanogenic archaea. *European Journal of Biochemistry* **2004,** *271* (1), 195-204.

7. Vignais, P. M.; Billoud, B., Occurrence, Classification, and Biological Function of Hydrogenases: An Overview. *Chemical Reviews* **2007,** *107* (10), 4206-4272.

8. Higuchi, Y.; Yasuoka, N.; Kakudo, M.; Katsube, Y.; Yagi, T.; Inokuchi, H., Single crystals of hydrogenase from Desulfovibrio vulgaris Miyazaki F. *Journal of Biological Chemistry* **1987,** *262* (6), 2823-2825.

9. Nivière, V.; Hatchikian, C.; Cambillau, C.; Frey, M., Crystallization, preliminary X-ray study and crystal activity of the hydrogenase from Desulfovibrio gigas. *Journal of Molecular Biology* **1987,** *195* (4), 969-971.

10. Rieder, R.; Cammack, R.; Hall, D. O., Purification and properties of the soluble hydrogenase from Desulfovibrio desulfuricans (strain Norway 4). *European Journal of Biochemistry* **1984,** *145* (3), 637-645.

11. (a) Ogata, H.; Hirota, S.; Nakahara, A.; Komori, H.; Shibata, N.; Kato, T.; Kano, K.; Higuchi, Y., Activation Process of [NiFe] Hydrogenase Elucidated by High-Resolution X-Ray Analyses: Conversion of the Ready to the Unready State. *Structure* **2005,** *13* (11), 1635-1642; (b) Volbeda, A.; Martin, L.; Cavazza, C.; Matho, M.; Faber, B. W.; Roseboom, W.; Albracht, S. P. J.; Garcin, E.; Rousset, M.; Fontecilla-Camps, J. C., Structural differences between the ready and unready oxidized states of [NiFe] hydrogenases. *Journal of Biological Inorganic Chemistry* **2005,** *10* (3), 239-249; (c) Lamle, S. E.; Albracht, S. P. J.; Armstrong, F. A., Electrochemical Potential-Step Investigations of the Aerobic Interconversions of [NiFe]-Hydrogenase from Allochromatium vinosum: Insights into the Puzzling Difference between Unready and Ready Oxidized Inactive States. *Journal of the American Chemical Society* **2004,** *126* (45), 14899-14909.

12. Fichtner, C.; Laurich, C.; Bothe, E.; Lubitz, W., Spectroelectrochemical Characterization of the [NiFe] Hydrogenase of Desulfovibrio vulgaris Miyazaki F†. *Biochemistry* **2006,** *45* (32), 9706-9716.

13. (a) van Gastel, M.; Stein, M.; Brecht, M.; Schröder, O.; Lendzian, F.; Bittl, R.; Ogata, H.; Higuchi, Y.; Lubitz, W., A single-crystal ENDOR and density functional theory study of the oxidized states of the [NiFe] hydrogenase from <i>Desulfovibrio vulgaris Miyazaki F.

Journal of Biological Inorganic Chemistry **2006,** *11* (1), 41-51; (b) Trofanchuk, O.; Stein, M.; Geßner, C.; Lendzian, F.; Higuchi, Y.; Lubitz, W., Single crystal EPR studies of the oxidized active site of [NiFe] hydrogenase from <i>Desulfovibrio vulgaris Miyazaki F. *Journal of Biological Inorganic Chemistry* **2000,** *5* (1), 36-44.

14. George, S. J.; Kurkin, S.; Thorneley, R. N. F.; Albracht, S. P. J., Reactions of H2, CO, and O2 with Active [NiFe]-Hydrogenase from Allochromatium vinosum. A Stopped-Flow Infrared Study†. *Biochemistry* **2004,** *43* (21), 6808-6819.

15. van der Zwaan, J. W.; Coremans, J. M. C. C.; Bouwens, E. C. M.; Albracht, S. P. J., Effect of 17O2 and 13CO on EPR espectra of nickel in hydrogenase from Chromatium vinosum. *Biochimica et Biophysica Acta (BBA) - Protein Structure and Molecular Enzymology* **1990,** *1041* (2), 101-110.

16. Ogata, H.; Lubitz, W.; Higuchi, Y., [NiFe] hydrogenases: structural and spectroscopic studies of the reaction mechanism. *Dalton Transactions* **2009,** (37), 7577-7587.

17. Armstrong, F. A.; Belsey, N. A.; Cracknell, J. A.; Goldet, G.; Parkin, A.; Reisner, E.; Vincent, K. A.; Wait, A. F., Dynamic electrochemical investigations of hydrogen oxidation and production by enzymes and implications for future technology. *Chemical Society Reviews* **2009,** *38* (1), 36-51.

18. Peters, J. W.; Lanzilotta, W. N.; Lemon, B. J.; Seefeldt, L. C., X-ray Crystal Structure of the Fe-Only Hydrogenase (CpI) from Clostridium pasteurianum to 1.8 Angstrom Resolution. *Science* **1998,** *282* (5395), 1853-1858.

19. Nicolet, Y.; de Lacey, A. L.; Vernède, X.; Fernandez, V. M.; Hatchikian, E. C.; Fontecilla-Camps, J. C., Crystallographic and FTIR Spectroscopic Evidence of Changes in Fe Coordination Upon Reduction of the Active Site of the Fe-Only Hydrogenase from

Desulfovibrio desulfuricans. *Journal of the American Chemical Society* **2001,** *123* (8), 1596-1601.

20. (a) Patil, D. S.; Moura, J. J.; He, S. H.; Teixeira, M.; Prickril, B. C.; DerVartanian, D. V.; Peck, H. D.; LeGall, J.; Huynh, B. H., EPR-detectable redox centers of the periplasmic hydrogenase from Desulfovibrio vulgaris. *Journal of Biological Chemistry* **1988,** *263* (35), 18732-8; (b) Pierik, A. J.; Hagen, W. R.; Redeker, J. S.; Wolbert, R. B. G.; Boersma, M.; Verhagen, M. F. J. M.; Grande, H. J.; Veeger, C.; Mutsaers, P. H. A.; Sands, R. H.; Dunham, W. R., Redox properties of the iron-sulfur clusters in activated Fe-hydrogenase from Desulfovibrio vulgaris (Hildenborough). *European Journal of Biochemistry* **1992,** *209* (1), 63-72; (c) Hatchikian, E. C.; Forget, N.; Fernandez, V. M.; Williams, R.; Cammack, R., Further characterization of the [Fe]-hydrogenase from Desulfovibrio desulfuricans ATCC 7757. *European Journal of Biochemistry* **1992,** *209* (1), 357-365.

21. (a) Razavet, M.; Borg, S. J.; George, S. J.; Best, S. P.; Fairhurst, S. A.; Pickett, C. J., Transient FTIR spectroelectrochemical and stopped-flow detection of a mixed valence {Fe(i)-Fe(ii)} bridging carbonyl intermediate with structural elements and spectroscopic characteristics of the di-iron sub-site of all-iron hydrogenase. *Chemical Communications* **2002,** (7), 700-701; (b) Fiedler, A. T.; Brunold, T. C., Computational Studies of the H-Cluster of Fe-Only Hydrogenases: Geometric, Electronic, and Magnetic Properties and Their Dependence on the [Fe4S4] Cubane. *Inorganic Chemistry* **2005,** *44* (25), 9322-9334.

22. Roseboom, W.; De Lacey, A.; Fernandez, V.; Hatchikian, E.; Albracht, S., The active site of the [FeFe]-hydrogenase from <i>Desulfovibrio desulfuricans . II. Redox properties, light sensitivity and CO-ligand exchange as observed by infrared spectroscopy. *Journal of Biological Inorganic Chemistry* **2006,** *11* (1), 102-118.

23. Pereira, A. S.; Tavares, P.; Moura, I.; Moura, J. J. G.; Huynh, B. H., Mössbauer Characterization of the Iron−Sulfur Clusters in Desulfovibrio vulgaris Hydrogenase. *Journal of the American Chemical Society* **2001,** *123* (12), 2771-2782.

24. De Lacey, A. L.; Fernández, V. M.; Rousset, M.; Cammack, R., Activation and Inactivation of Hydrogenase Function and the Catalytic Cycle: Spectroelectrochemical Studies. *Chemical Reviews* **2007,** *107* (10), 4304-4330.

25. Lubitz, W.; Reijerse, E.; van Gastel, M., [NiFe] and [FeFe] Hydrogenases Studied by Advanced Magnetic Resonance Techniques. *Chemical Reviews* **2007,** *107* (10), 4331-4365.

26. (a) Liu, Z.-P.; Hu, P., A Density Functional Theory Study on the Active Center of Fe-Only Hydrogenase: Characterization and Electronic Structure of the Redox States. *Journal of the American Chemical Society* **2002,** *124* (18), 5175-5182; (b) Zhou, T.; Mo, Y.; Zhou, Z.; Tsai, K., Density Functional Study on Dihydrogen Activation at the H Cluster in Fe-Only Hydrogenases. *Inorganic Chemistry* **2005,** *44* (14), 4941-4946.

27. Pneumatikakis, G.; Hadjiliadis, N., Complexes of Cysteine and Cysteinemethylester with Pd(II) and Pt(II). *Journal of Inorganic and Nuclear Chemistry* **1979,** *41* (3), 429-435.

28. Crabtree, R. H., The Organometallic chemsitry of the transition metal **2009,** *5th Ed,* 4-5.

29. Nguyen, D. H., Ph. D. Dissertation: Synthesis and characterization of nickel thiolate complexes as a model of the active site of [NiFe] hydrogenase enzymes, *Stony Brook Univeristy* **1997**.

30. Eisch, J. J.; Gopal, H.; Kuo, C. T., Studies on nonpyridinoid azaaromatic systems. 7. Synthesis and tautomeric character of cyclopenta[c]quinoline (benzo[c][2]pyrindine). *The Journal of Organic Chemistry* **1978,** *43* (11), 2190-2196.

31. Koh, j. T.-T., *PCT Int. Appl. 2008013791* **2008**.

32. (a) Hsu, H.-F., Ph. D. Dissertation: Synthesis and characterization of iron complexes of tris thiolate phosphine tripodal ligands., *Stony Brook Univeristy* **1997**; (b) Franolic, J. D., Ph. D. Dissertation: Synthesis, structure and reactivity of transition metal thiolate dimers., *Stony Brook Univeristy* **1993**; (c) Lu, G., Ph. D. Dissertation: Metal-thiolate complexes for metal cysteine centers in metalloproteins: the role of the second coordination sphere interaction., *Stony Brook Univeristy* **2010**.

Appendix

Table 2. Crystal data and structure refinement for $Fe^{II}[PS3(o\text{-}Ph)]_2$.

Empirical formula	C72 H48 Fe P2 S6	
Formula weight	1223.25	
Temperature	100 K	
Wavelength	0.71073 Å	
Crystal system	Monoclinic	
Space group	C 2/c	
Unit cell dimensions	a = 23.3401(9) Å	α= 90°.
	b = 10.5398(3) Å	β= 106.662(4)°.
	c = 24.1134(9) Å	γ = 90°.
Volume	5682.8(3) $Å^3$	
Z	4	
Density (calculated)	1.430 Mg/m^3	
Absorption coefficient	0.588 mm^{-1}	
F(000)	2528	
Crystal size	0.3 x 0.2 x 0.2 mm^3	
Theta range for data collection	3.19 to 29.70°.	
Index ranges	-29<=h<=30, -9<=k<=14, -30<=l<=30	
Reflections collected	22020	
Independent reflections	6987 [R(int) = 0.0876]	
Completeness to theta = 29.70°	86.6 %	
Refinement method	Full-matrix least-squares on F^2	
Data / restraints / parameters	6987 / 0 / 366	
Goodness-of-fit on F^2	1.033	
Final R indices [I>2sigma(I)]	R1 = 0.0520, wR2 = 0.1102	
R indices (all data)	R1 = 0.0774, wR2 = 0.1271	
Largest diff. peak and hole	0.915 and -0.658 e.$Å^{-3}$	

Table 3. Crystal data and structure refinement for S-2-benzylphenyl-diethyldithiocarbamic acid.

Empirical formula	C17 H19 N S2	
Formula weight	301.45	
Temperature	293(2) K	
Wavelength	0.71073 Å	
Unit cell dimensions	a = 12.6251(3) Å	a= 90°.
	b = 8.6297(2) Å	b= 110.962(3)°.
	c = 16.2267(4) Å	g = 90°.
Volume	1650.91(7) $Å^3$	
Z	4	
Density (calculated)	1.213 Mg/m^3	
Absorption coefficient	0.313 mm^{-1}	
F(000)	640	
Theta range for data collection	3.46 to 29.69°.	
Index ranges	-16<=h<=15, -11<=k<=11, -21<=l<=22	
Reflections collected	27159	
Independent reflections	4350 [R(int) = 0.0237]	
Completeness to theta = 29.69°	93.1 %	
Refinement method	Full-matrix least-squares on F^2	
Data / restraints / parameters	4350 / 0 / 181	
Goodness-of-fit on F^2	1.061	
Final R indices [I>2sigma(I)]	R1 = 0.0398, wR2 = 0.1037	
R indices (all data)	R1 = 0.0524, wR2 = 0.1138	
Largest diff. peak and hole	0.181 and -0.385 $e.Å^{-3}$	

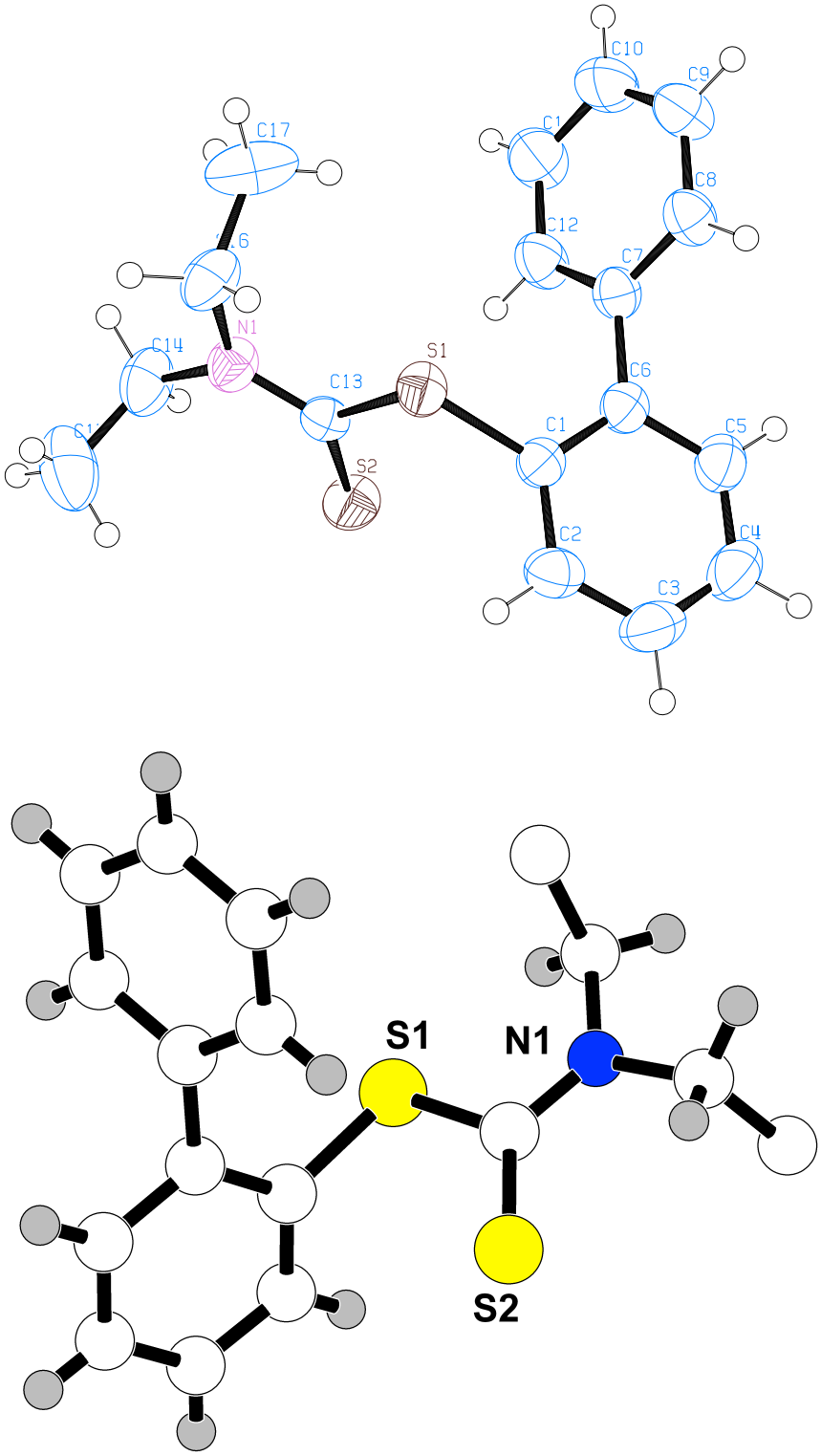

Figure 17. CHARON and Ortep Structure of S-2-benzylphenyl-diethyldithiocarbamic acid